Superstructure Evolution in Poly(ethylene terephthalate) during Uniaxial Deformation above Glass Transition Temperature

Daisuke Kawakami,[†,‡] Shaofeng Ran,[†] Christian Burger,[†] Carlos Avila-Orta,[⊥,†] Igors Sics,[†] Benjamin Chu,[†] Benjamin S. Hsiao,*[,†] and Takeshi Kikutani*[,§]

Department of Chemistry, Stony Brook University, Stony Brook, New York 11794-3400; Research and Management Division, Toray Industries, Inc., Shiga Plant, 1-1-1 Sonoyama, Otsu, Shiga 520-8558, Japan; and Department of Organic and Polymeric Materials, Tokyo Institute of Technology, O-okayama, Meguro-ku, Tokyo 152, Japan

Received December 4, 2005; Revised Manuscript Received February 4, 2006

ABSTRACT: The evolution of superstructure and its relationship with the phase transition during uniaxial deformation of poly(ethylene terephthalate) (PET) at temperatures (90 and 100 °C) above its glass transition temperature were investigated by in-situ small-angle X-ray scattering (SAXS) and wide-angle X-ray diffraction (WAXD). It appears that deformation at lower temperatures enhances the metastability of mesophase but narrows the strain window for phase transition. Very similar superstructure evolution pathways were observed at both temperatures. In zone I (the plastic deformation zone), WAXD did not show any crystal diffraction peak; however, SAXS exhibited an equatorial streak at the later stage, indicating the formation of a microfibrillar structure. Strain hardening took place in zone II, which could be categorized in two substages. In zone II-a, SAXS showed an X-shaped pattern that coincided with the appearance of crystal diffraction peaks in WAXD. The initial X-shaped patterns possessed strong intensity near the beam stop; the later patterns exhibited a scattering maximum that shifted toward larger angles with increasing strain. Results indicated the formation of a tilted lamellar structure within the microfibrils in conjunction with lamellar insertion. In zone II-b, oval spots appeared at the edges of the X-shaped pattern, which essentially became four-point. In this stage, the crystallinity still increased linearly with strain, but the invariant gradually reached an asymptotic value, indicating that lamellar insertion took place at a slower rate. In the final strain-hardening zone (III), the load became linear with strain even though crystallization was reduced. The equatorial long period was found to decrease drastically, suggesting that some microfibrils were split. In addition, a two-point pattern appeared near the central streak, corresponding to a periodic structure with long period of 100 nm. The formation of such a large layered structure and the microfibrillar splitting can be attributed to structural defects such as kinks in microfibrils.

1. Introduction

Recently, in-situ studies during uniaxial deformation of poly(ethylene terephthalate) (PET) have been carried out by many laboratories.[1−13] Some new insights into the structure and property relationships in this widely used thermoplastic material have been obtained. In brief, PET can be considered as a "marginal" liquid crystalline polymer.[3] Its mesomorphic transitions are not obvious in the isotropic state but become distinct in the oriented state, in which the mesomorphic phase appears to be the precursor phase for crystallization.[1−13] In our earlier study,[3] we found that the superstructure formation took place during deformation below the glass transition temperature (T_g), and the evolution process is closely related to multiple phase transitions involving amorphous, nematic, smectic, and crystalline phases. We used the term "superstructure" instead of "morphology" to emphasize that the observation of the large-scale structure formation (from 10 to 100 nm) was made by small-angle X-ray scattering instead of by typical microscopic techniques. In the current study, we continued the investigation of this subject with an emphasis on superstructure formation and its relationship with the phase transition during uniaxial deformation at temperatures (e.g., 90 and 100 °C) above the glass transition temperature. The study was carried out by simultaneous 2D small-angle X-ray scattering (SAXS) and wide-angle X-ray diffraction (WAXD) techniques using synchrotron radiation.

The behavior of plastic deformation (i.e., the true stress can remain constant with increasing strain) near the glass transition in PET has been well recognized and routinely used in the shaping of varying products (e.g., films and fibers). The window of plastic deformation in PET is directly related to temperature: at low temperatures (e.g., below T_g), the window is narrow and sometimes nonexistent; at high temperatures (e.g., above T_g), the window is relatively large. In our previous study of PET deformation below T_g,[3] we found that the unique mechanical responses in the plastic deformation zone and subsequent strain-hardening zones are related to complicated phase transitions, involving amorphous, nematic, smectic, and crystalline phases, which are also accompanied by evolution of varying superstructures (e.g., microfibrils and subsequent lamellar structures within microfibrils). In this context, the current state of understanding in the superstructure formation in PET, induced by uniaxial stretching, will be briefly reviewed below. (We note that the phenomenon of deformation-induced mesophase has recently been discussed by us and many others[1−20] and thus will not be repeated here.)

The structural change in cold drawn PET films under annealing has been investigated by Asano et al.[5] They reported that the transition from the nematic phase to the triclinic

† Stony Brook University.
‡ Toray Industries, Inc.
§ Tokyo Institute of Technology.
⊥ Current address: Centro de Investigación en Química Aplicada, Saltillo, COAH, México 25100.
* To whom correspondence should be addressed. Hsiao: Tel 631-632-7793; Fax 631-632-6518, e-mail bhsiao@notes.cc.sunysb.edu. Kikutani: Tel 81-3-5734-2468; Fax 81-3-5734-2876; e-mail tkikutan@o.cc.titech.ac.jp.

10.1021/ma052589y CCC: $33.50
Published on Web 03/15/2006

crystalline phase took place through the smectic A phase (with a characteristic *d*-spacing of 1.07 nm), where the formation of smectic A phase was correlated with the occurrence of a layered structure (with a long period of about 10 nm) shown as a two-bar pattern in SAXS. Our group also investigated the mechanism of structural formation in amorphous PET during uniaxial deformation both above its T_g (90 °C)[1,2] and below T_g (70 °C).[3] Results above T_g indicated that the structural development could be categorized into three zones, designated as I, II, and III. In zone I, the oriented mesophase in the microfibrillar superstructure is induced by strain, where the applied load remains about constant. In zone II, lamellar crystallization is initiated from the mesophase through nucleation and growth, where the load starts to increase marking the beginning of the strain-hardening region. In zone III, the stable lamellar crystal growth process is facilitated by strain-induced orientation until the breaking of the sample, where the ratio between load and strain remains about constant. The study below T_g showed that the appearance of metastable mesomorphism was enhanced under uniaxial deformation, where transitions of a series of mesophases occurred, including nematic, quasi-smectic A, smectic C, and triclinic crystalline structure, all within the microfibrillar superstructure. The formation of the smectic phase was definitely related to the initiation of a lamellar structure, as suggested by Asano et al., but it appeared to have a periodicity (ca. 100 nm) much larger than that of a typical lamellar structure in the solid phase (ca. 10 nm).

Shimizu et al. investigated the initial structural formation of PET fibers spun at various spinning speeds (above 5000 m/min) by SAXS.[21,22] The scattering pattern exhibited an X-shaped feature at 5000 m/min, and it shifted to an inverted triangular shape with intensity spreading toward the meridional direction at higher speeds. They proposed a tilted block alignment, consisting of microfibril, to explain this superstructure. Kubo et al. studied the structure evolution of PET melt under flow by in-situ small-angle light scattering.[23] They found that in Ge-catalyzed PET molecular orientation increased along the flow direction; flow-induced crystallization took place rather suddenly at a Hencky strain of about 2, where crystalline lamellae grew perpendicularly with respect to the oriented chains. The periodicity between the optical lamellar texture was about 2 μm. Recently, Mahendrasingam et al. performed time-resolved X-ray measurements of PET during deformation at 90 °C (above the T_g) using the step drawing technique.[13] They observed interesting SAXS patterns with four-point off-axis scattering and a very weak equatorial streak prior to crystallization, from which they proposed the smectic phase composed of microfibrillar structure. Unfortunately, they did not correlate the structure evolution with the mechanical response during deformation.

In this study, we carried out in-situ SAXS/WAXD measurements of PET during uniaxial deformation at two different temperatures (i.e., 90 and 100 °C) about its T_g (ca. 80 °C). The work was emphasized on the SAXS analysis, which yielded in-situ information about the super structure evolution. The complementary WAXD data were also collected to confirm the phase information. A relatively slow deformation rate was utilized to obtain the scattering patterns with sufficient signal-to-noise ratios for detailed X-ray analyses. A particular focus was also placed on the initial stage of structure formation and its relationship with the mechanical response. The categorization of super structure formation (i.e., in different zones: I, II, and III) was employed to evaluate a previously proposed structure model [3] derived mainly from the WAXD study of PET at 70 °C just below its T_g. This model was carefully verified and modified using mainly the SAXS results from PET deformation above its T_g.

2. Experimental Section

2.1. Samples Preparation. The PET samples were specially prepared by Toray Co. Ltd. in Japan, as described in detail previously.[3] In brief, its weight-average molecular weight (M_w) was 35 000 g/mol, and the polydispersity (M_w/M_n) was about 2.0. Minimum amounts of antimony and phosphate were used to prepare this sample, whereby the sample could be viewed as a pure polymer that would not decompose under high molding temperatures. The pellet sample was molded into a dumbbell shape at 270 °C followed by rapid quenching to 0 °C with ice water. The drawing part of the dumbbell sample was 25 mm length, including taper part, 6 mm width, and 1 mm thickness. The molded samples were completely amorphous, having no detectable crystallinity by WAXD.

2.2. Experimental Procedures. During in-situ deformation for X-ray measurements, the sample was mounted in the environmental chamber of the modified Instron stretching apparatus (model 1440),[24] which was heated by hot air. The sample was equilibrated in the heated chamber for 3 min at the desirable temperature (i.e., 90 and 100 °C) before the engagement of tensile deformation. The deformation process was continued until the sample broke. The load−strain curve was recorded simultaneously during the collection of SAXS and WAXD signals. Measurements were also carried out at 90 and 100 °C without deformation for 40 min, which was the maximum deformation time, in the same manner as the studies under deformation. An average WAXD image was collected for each measurement (i.e., all images were summed up and then divided by the number of the images taken), which was used as a reference of the amorphous phase. (No crystallization was observed in the samples at either temperature 90 or 100 °C, even in the last images after 40 min annealing.)

2.3. Synchrotron X-ray Measurements. Synchrotron X-ray measurements were carried out at the X27C beamline in the National Synchrotron Light Source (NSLS), Brookhaven National Laboratory (BNL). The wavelength of this beamline was 1.366 Å. A three-pinhole collimator system was used to reduce the beam size to 0.6 mm in diameter.[25] The modified Instron apparatus permitted the symmetrical stretching, which ensured that the focused X-ray beam always illuminated on the same sample position during deformation. The chosen deformation rate was 5 mm/min (i.e., 20% strain/min), and the experiment was carried out at temperatures of 90 and 100 °C for SAXS and 100 °C for WAXD. 2D patterns were accumulated over the collection period of 60 s for SAXS and 20 s for WAXD using a CCD X-ray detector (MAR USA). The sample-to-detector distance was 1783 mm for SAXS and 119.4 mm for WAXD. The diffraction angle in WAXD was calibrated by using a polypropylene standard from our laboratory and an Al_2O_3 standard from the National Institute of Standards and Technology (NIST). A silver behenate (AgBe) standard was used to calibrate the scattering angle in SAXS. We note that the high intensity of the synchrotron X-rays made it possible to collect the SAXS/WAXD patterns during stretching in real time without holding.

2.4. X-ray Data Analysis. WAXD studies above T_g have been reported previously;[1,2] the same procedure was used in this study and will not be repeated here. For SAXS analysis, the contribution of air scattering was removed from each measured image using the transmitted beam intensity detected by a pin-diode beam stop as a reference.[26] Fiber symmetry around the stretching axis was assumed for the SAXS study,[3] and the invariant was determined using the following procedures.[27] The two-dimensional (2D) SAXS pattern was first projected onto the equatorial axis to obtain integrated equatorial intensity profile, $I_e(s)$ (s is the scattering vector, defined as $s = 2 \sin \theta/\lambda$, where 2θ is the scattering angle and λ is the wavelength of X-rays). This intensity profile was assumed to have the $1/s^3$ dependence at large scattering angles, and the scattering data were fitted with a corresponding function to extrapolate the missing region at large s. The invariant (Q) was

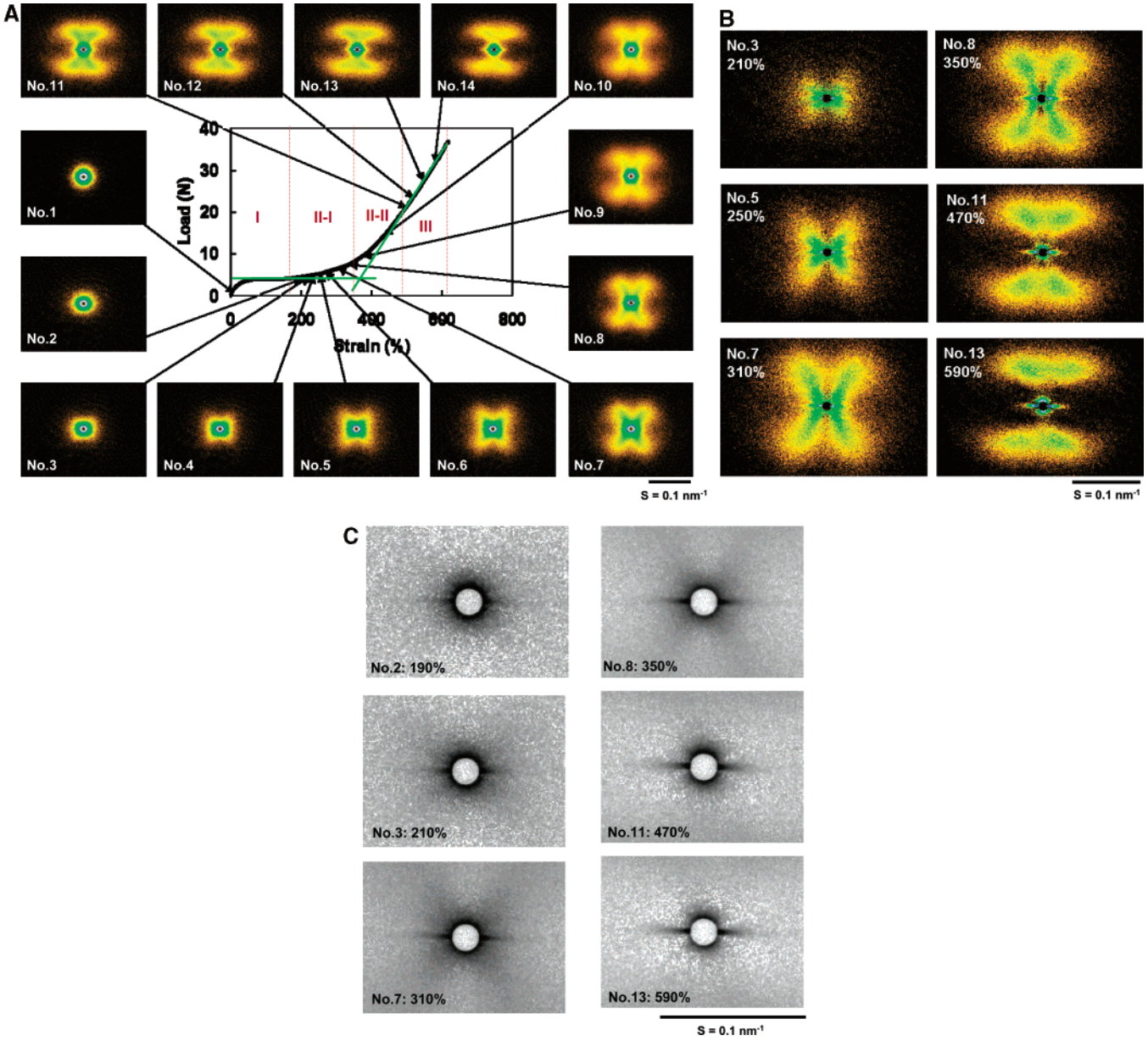

Figure 1. (A) Load−strain curve and selected SAXS images of the amorphous PET sample during drawing at 100 °C. (B) Anisotropic contributions of selected SAXS images. (C) The visually enhanced equatorial streak feature of selected SAXS image.

estimated as the area underneath the integrated equatorial intensity profile ($Q = 2\pi\int_0^\infty I_e(s)\,ds$), which was normalized by the beam fluctuations and the sample thickness. The long period was evaluated from Bragg's law, L_b ($= 1/s_{max}$), where s_{max} represents the peak position in the Lorentz correlated scattering plot, i.e., Is^2 vs s. The long periods estimated by equatorial and meridional projection (L_e and L_m, respectively) were used to calculate the diagonal long period ($L = (L_e^2 + L_m^2)^{1/2}$).

3. Results and Discussion

From our earlier in-situ WAXD studies during deformation of an amorphous PET sample, both face-on and edge-on measurements confirmed that the formed anisotropic structure possessed a cylindrical symmetry.[1−3] This assumption significantly simplified the data analysis schemes. In this work, two different temperatures were used: 90 and 100 °C, both are above T_g. (Here we define T_g as the temperature at the inflection point of the heat capacity change in DSC thermogram measured at a heating rate of 18 °C/min under a dry nitrogen atmosphere; T_g determined in such a way was 78 °C.) Results from 100 °C will be presented first, and results from 90 °C will be discussed next as deformation at lower temperatures in PET generally yields more complicated mesomorphic transitions.[3] When a thorough comparison between the structural changes at different temperatures is made, we also attempt to correlate the structure evolution and the mechanical property. Resulting structure changes are evaluated again on the basis of categorization of three zones: plastic deformation zone (zone I), strain hardening zone (zone II), and linearly load developing zone (zone III), derived from our earlier studies[1−3] to check its universality.

3.1. Deformation at 100 °C. The load−strain (LS) curve during uniaxial deformation of an amorphous PET sample at 100 °C and selected as-measured SAXS images are shown in Figure 1A. The scattering contribution from nondeformed sample was subtracted from some critical images during the zone transition, taking into consideration of the sample thickness. Selected subtracted images are shown in Figure 1B. Another set of enlarged SAXS images to illustrate the evolution of central scattering streak feature is shown in Figure 1C. The corre-

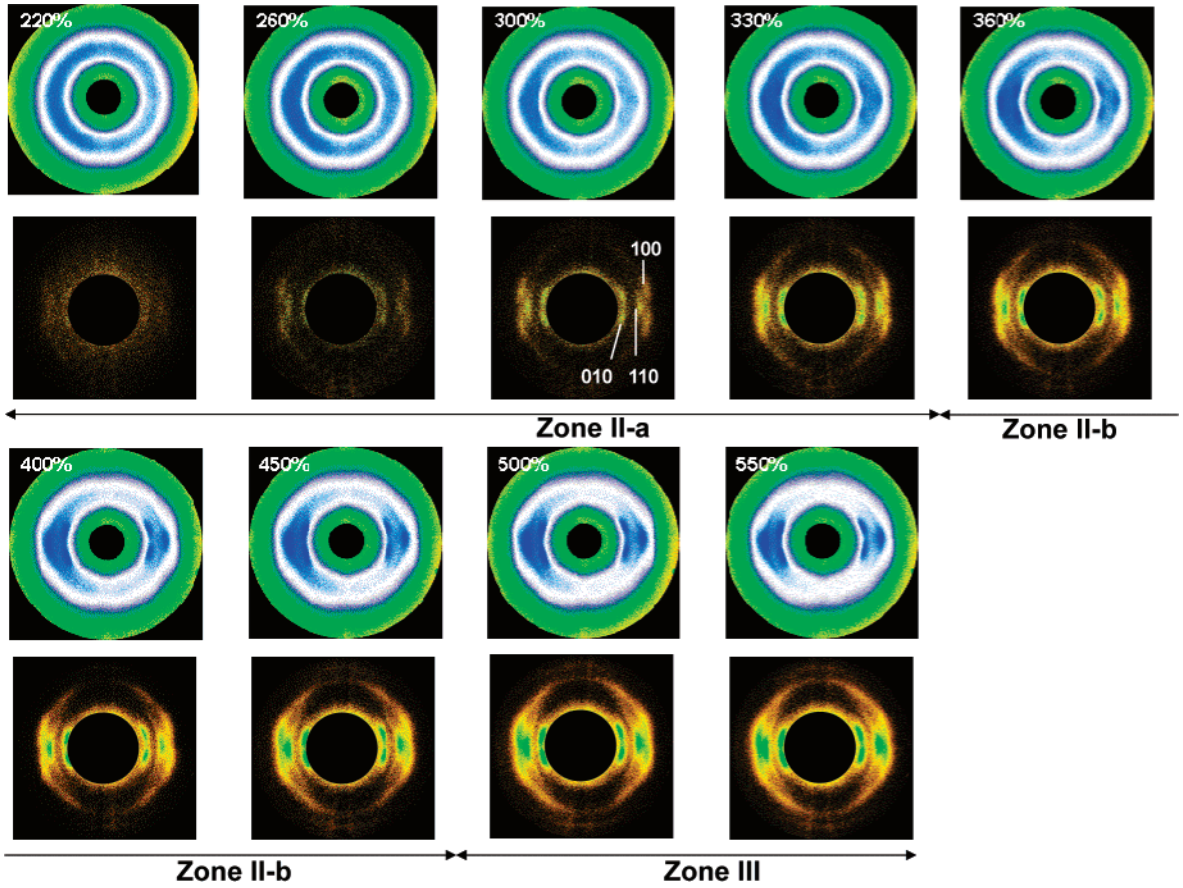

Figure 2. Selected WAXD images of the amorphous PET sample drawn at 100 °C: (upper) as measured patterns; (lower) anisotropic contributions of the images.

sponding as-measured WAXD patterns and subtracted anisotropic images (i.e., with the removal of amorphous contribution) are illustrated in Figure 2. The number at the upper left of each image represents the strain at which the image was taken. The peak assignments were given on the image of 300% strain; the zones were also indicated. The analytical methods of WAXD were described in detail elsewhere [1,2] These results are discussed in the categorization of three zones as follows.

3.1.1. Zone I: Plastic Deformation Zone (0−170% Strain). This is the region often referred to as the plastic flow region exhibiting properties similar to the flow of a viscous fluid,[28−30] where the strain increases without any increase in stress. In other words, the yield plateau for an "ideal" plastic in the concept of plasticity is achieved. Beyond the yield plateau, strain hardening occurs, where the material stiffens resulting in an increase in modulus. It was found that the plastic flow region in amorphous PET above T_g was significantly broader than that below T_g.[3] In the major portion of zone I, no distinct scattering or diffraction feature was observed by SAXS and WAXD (Figures 1 and 2). This observation can be explained by the stress−optical rule. The stress−optical coefficient of PET is around 4.8 GPa^{-1}, and the stress applied in this region was around 1 MPa (3 N/6 mm^2 $\times$ 2.7). Therefore, the corresponding birefringence was around 0.005, and the orientation factor was about 0.025, which is too small to induce any structure change. In the late stages of zone I (i.e., near 170%), SAXS exhibited a distinct equatorial streak. Such a scattering streak might not be resulted from the void scattering because the quenched deformed samples did not show any void structure by electron microscopy or whitening under visible light. The streak appearance thus might indicate the formation of a microfibrillar structure, which occurred before crystallization since no WAXD diffraction was seen at the same strain. A similar phenomenon under deformation has also been reported by other research groups.[31−37] For example, Zachmann et al.[31] as well as Schultz and Hsiao et al.[32,33] carried out in-situ SAXS and WAXD studies on the melt spinning of poly(vinylidene fluoride) (PVDF) and polyethylene (PE). They reported that the SAXS signal appeared prior to crystallization detected by WAXD, indicating that density fluctuations take place before crystallization. Ryan et al. also observed this phenomenon during extrusion of isotactic polypropylene (iPP) and proposed that it could be attributed to spinodal-decomposition-induced phase separation, where the amorphous phase underwent modulated density fluctuations.[34,35] The concept of spinodal decomposition as the driving force to induce crystallization was first proposed by Petermann et al.[38,39] and followed by Imai et al.,[40−45] who have extensively studied the cold crystallization of PET at the quiescent state. They argued that density fluctuations via route of spinodal decomposition form the precursor state for crystallization. Recently, our group also observed the phenomenon of SAXS before WAXD during step-shear deformation of iPP[36] and PE[37] melts, which was explained by sequential growths of shish and kebab structures instead of spinodal decomposition.

Although we are not sure whether the mechanism of spinodal decomposition is truly responsible for the density fluctuations observed at the initial stages of PET during deformation above T_g, we anticipate that there are two possible pathways for the evolution of molecular structure in this zone. In the first pathway, mechanical extension of the sample induces rotation of chemical bond in molecules, where all chains can be extended locally as well as macroscopically. Because the molecular

relaxation time is proportional to the molecular weight by a power of 3.4, short molecular weight chains would maintain its undeformed state during deformation in a relatively slow rate, while long molecular weight chains can be stretched selectively.[46] Another pathway is that chains have strong inter- or intramolecular interactions, such as dipole−dipole (between C═O's) and/or induced polarized interactions (between benzene molecules), which form reversible cross-links that can induce molecular orientation and extension locally. The reversible interactions may break, while in some instances, the interactions let molecular chains become closer. As a result, the opportunity for chains to interact increases, and the number of the interactions increases as deformation. But the amount, as well as the ordering of these deformed chains, may be too small to be detected by WAXD techniques.

3.1.2. Zone II: Strain Hardening Zone (170−470% Strain). In Figure 1, the strain hardening zone II began at a strain value about 170%, where the nonlinear load increase was caused by development of ordered structures. From the standpoint of structure formation, this zone can be further divided into two subzones, II-a and II-b, as follows.

Zone II-a (170−350% Strain). Figure 1B shows selected SAXS patterns in this subzone; all exhibit an X-shaped scattering feature. The scattering arms were short in the early stages of this zone, and they extended outward with the cross angle being almost constant (i.e., 25°) at larger strains. No scattering maximum was detected on the scattering arm at strains up to 310%, and if there was any, it was within the beam stop (i.e., larger than 100 nm). At strains above 310%, the SAXS pattern became four-point with clear scattering maximum. The long axis of each scattering peak exhibited the principal direction along the arm of the X-shaped pattern at the beginning of this subzone. It was interesting to note that the occurrence of the X-shaped pattern (Figure 1B) coincided with the detection of peak splitting of (100) and (010) reflections in WAXD, as seen in Figure 2. The splitting of these two peaks indicates the tilting of crystallites along the stretching axis. The tilt angle was about 15° from the evaluation of (100) and (010) peaks near the equator. We argue that the structures associated with the X-shaped and the four-point patterns are qualitatively the same despite their difference in appearance, and they are related to the crystallization process in oriented PET. The four-point pattern in PET has been explained by the concept of microfibril,[21,22,47] which includes two possible arrangements. In one arrangement, crystals in the microfibrils are lamellae with tilted arrangement (i.e., inclined end-face),[48,49] while there is no correlation between the neighboring microfibrils. In another arrangement, the lamellae in the neighboring microfibrils are correlated without being tilted[21,22,47] (the so-called chessboard model). Both arrangements can generate the four-point pattern, and the real structure may be the mixture of the two. However, we favor the tilted arrangement in zone II-a, based on the crystal structure changes under deformation from our earlier in-situ WAXD studies[1−3] and some previous reports.[4,5] The initial structure for triclinic structure has been revealed to be an oriented smectic structure.[1−12] In the smectic structure, benzene molecules form rows perpendicularly to the mechanical axis.[3,5] When the smectic transforms to triclinic, the oriented molecules slip one another, resulting in tilting alignment of benzene molecules against the stretching axis.[3,4] Asano reported that the two-bar pattern appeared in SAXS when the smectic structure was seen in WAXD, suggesting the domain size of smectic structure is in the range of 10 nm. Moreover, they proposed the tilting end-face domain of triclinic structure. Our results are consistent with the concept of slipping mechanism of molecular chains in the smectic structure, leading to the tilted end-face domain in the subsequent triclinic structure.

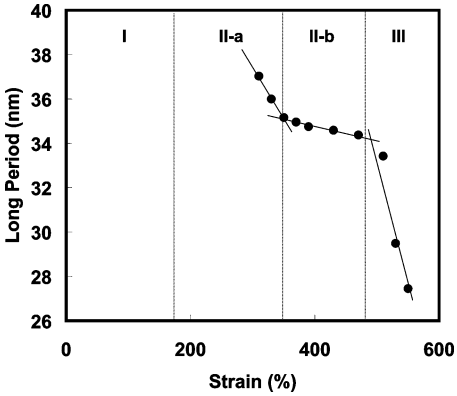

Figure 3. Long period change from the SAXS pattern during drawing at 100 °C.

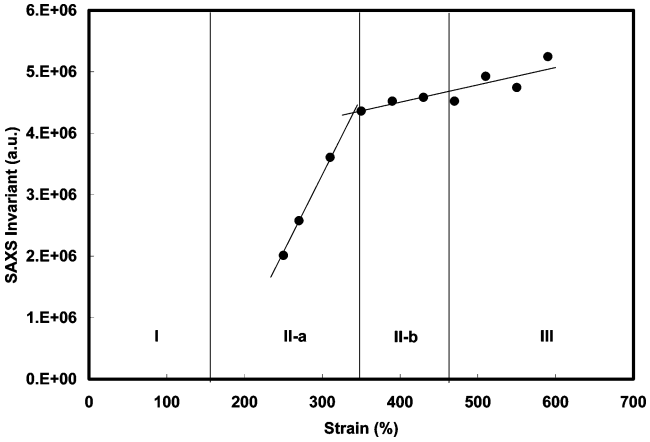

Figure 4. Invariant change from the SAXS pattern during drawing at 100 °C.

The assumption of the microfibrillar structure is consistent with the persistent appearance of equatorial streak in SAXS, whereby microfibrils are aligned parallel to the stretching direction. It was found that the tilt angle of the X-shaped scattering pattern was about constant (i.e., 25°−30° with respect to the fiber axis) in this subzone, but the periodicity of the lamellae decreased with strain. At low strains, it was difficult to determine the long period since the scattering maximum appeared to be buried within the beam stop or the wide distribution of long period. At higher strains (e.g., in the range of 310−350%), the scattering maximum was clearly seen, and it shifted toward higher angles at higher strains, indicating the formation of a denser lamellar structure. Figure 3 illustrates the long period change (determined from the average long period as defined earlier) with strain (after 310% strain). In zone II-a, the long period was found to decrease rapidly (e.g., 38 nm at 310% and 35 nm at 350%), which can be explained by the conventional nucleation mechanism; i.e., more nucleating sites are generated at higher strains (this mechanism is often termed lamellar insertion), leading to the reduction of long period.

Figure 4 illustrates the SAXS invariant as a function of strain. In zone II-a, the invariant was found to increase linearly with strain (the invariant at strain 350% was approximately twice of that at 250%), which is similar to the crystallinity change that will be discussed next. This suggests that the origin for the X-shaped or four-point pattern in SAXS is mainly due to the development of crystalline structure, not related to the mesomorphic transition as found in the case of deformation below the glass transition temperature.[3] Results obtained from in-situ

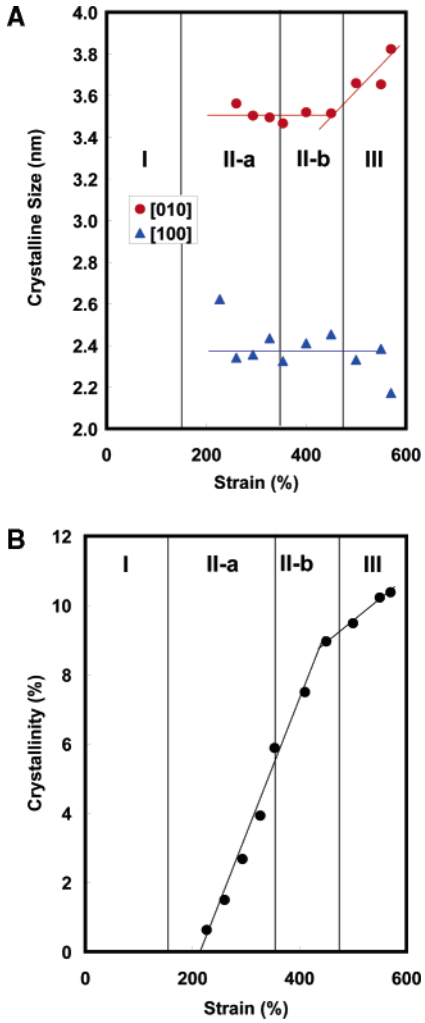

Figure 5. (A) Crystalline size estimated from (100) and (010) reflections of the sample during drawing at 100 °C. (B) Crystallinity change during drawing at 100 °C.

WAXD images (Figure 2) are shown in Figure 5, where Figure 5A illustrates the crystal sizes associated with the crystalline (100) and (010) reflections (the (−103) reflection could not be used because it was too weak), while Figure 5B illustrated the crystallinity change with strain. In Figure 5A, the estimated crystalline size along the plane normal of the (100) reflection was about 2.4 nm and of the (010) reflection was about 3.5 nm. The dominance of the size for the (010) reflection is due to the stronger dipole−dipole interactions of C═O than the induced polarized interactions of benzene molecules.[1−3] The constant crystal size in zone II-a indicates that the perfection or the "growth" of the lamellae is minimal; thus, the linear crystallinity increase is mainly due to the formation of new lamellae through the lamellar insertion mechanism. The crystallinity at strain 350% was also found to be about 2.5 times that at 250%, similar to the change in the SAXS invariant. This can be explained as follows. The invariant $Q = C\phi_c\phi_a(\rho_c - \rho_a)^2$, where C is a constant, ϕ_c is the volume fraction of the crystalline phase, ϕ_a is the volume fraction of the amorphous phase, and $(\rho_c - \rho_a)$ is the electron density contrast. At low crystallinity, the product of $\phi_c\phi_a$ is directly proportional to ϕ_c, which would be the case in zone II; while at high crystallinity, this relationship will not hold. It was interesting to note that all crystals formed in zone II-a were highly oriented (Figure 2), and no detectable oriented noncrystalline fraction (or mesophase) could be observed—Figure 2 revealed no meridional (001′) peak from the smectic structure or equator scattering peak from the nematic structure. This indicated that the transformation from the oriented mesomorphic phase to oriented crystalline phase is quite rapid above T_g due to the higher chain mobility, which is quite different from the case below T_g where several metastable mesophases were seen.

Zone II-b (350−470% Strain). The zone between 350% and 470% strains was defined as zone II-b, where the relationships between the structural parameters and strain were found to deviate from those in zone II-a (e.g., the change of long period was found to slow down considerably in zone II-b, as seen in Figure 3). Although the general mechanism of crystallization in this subzone appeared to be the same as that in zone II-a, the deviations of the structural parameters are notable and can be described as follows. All SAXS patterns in this subzone exhibited a four-point scattering feature. However, the principal axis of the scattering peak in these four-point patterns became parallel to the equatorial direction (e.g., Figure 1, no. 8), which was different from those in zone II-a. Nevertheless, there was no change in the equatorial streak (Figure 1C). The rate of long period reduction, determined from the position of the scattering maximum, was found to decrease in this subzone. The long period still showed a negative slope with strain, but the reduction rate was several times smaller than that in zone II-a (Figure 3). In addition, the increase of the invariant was found to decrease significantly but still exhibited a linear slope with strain (Figure 4). On the other hand, the corresponding rate of the crystallinity increase was found to be the same as that in zone II-a (Figure 5B).

The above findings suggested that, although the crystallinity continued to increase with strain in zone II-b, the addition of the new crystallites did not significantly change the basic lamellar structure formed in zone II-a. There are two possibilities for such a behavior. One is due to the mechanism of lamellar thickening, which would result in the continuous increases of crystallinity and (possible) scattering invariant. (This depends on the value of ϕ_c because Q is proportional to the product of $\phi_c(1 - \phi_a)$ and has the maximum value at $\phi_c = 50\%$.) However, the long period should remain constant in this case, which was not seen. Thus, this scenario is not favorable. Another possibility is due to the continuation of lamellar insertion as in zone II-a. Since the relatively dense lamellar structure is already formed after zone II-a, the addition of new lamellae can only reduce the average long period in a moderate rate. Such a mechanism would increase the total invariant, but at a slow rate. This may be the more likely scenario. It is interesting to note that the rotation of the four point pattern from zone II-a to zone II-b was not related to the crystal orientation. This is because the azimuthal dependencies of the (010), (−110), and (100) reflections were not changed during the transition. Thus, the change of the four-point pattern is primarily due to the alternation of superstructure, such as the formation of the "chessboard" arrangement.

3.1.3. Zone III: Linear Load−Strain Relationship (>470%). In zone III, a large linear decrease in the long period was seen (Figure 3), having a slope more negative than those in zone II-a and zone II-b. To further examine this behavior, we also evaluated both equatorial and meridional long periods separately. The meridional long period was 16 nm at the beginning of zone III and was 14 nm just before the sample breakage. On the other hand, the equatorial long period changed dramatically from 31 to 23 nm. Thus, the decrease of equatorial long period was mainly due to the change of long period seen in Figure 3. This observation is consistent with the hypothesis put forth by Shimizu et al.,[21] who argued that the microfibril structure can be divided by the slipping mechanism under high strains.

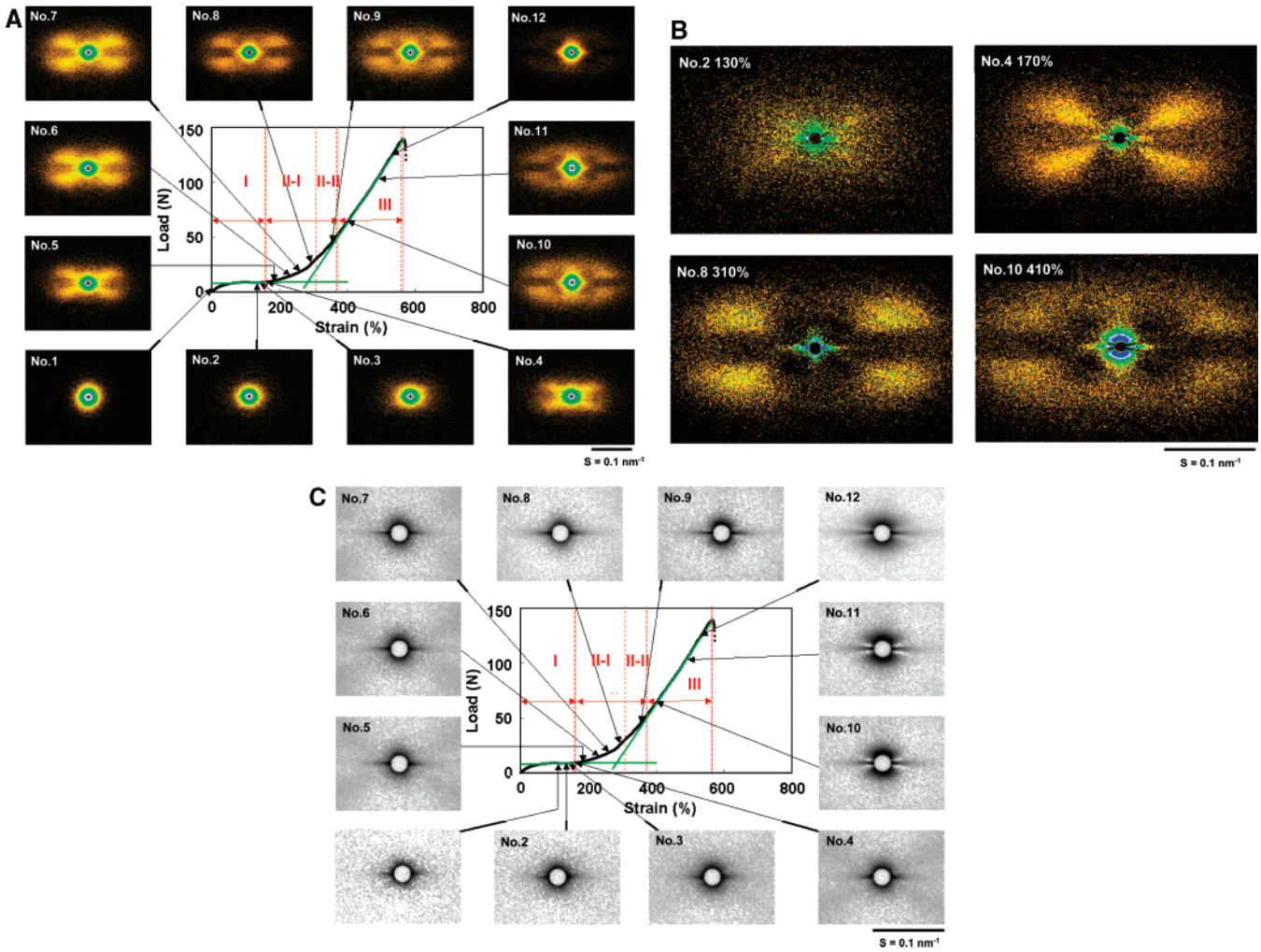

Figure 6. (A) Load−strain curve and selected SAXS images and of the sample during drawing at 90 °C. (B) Anisotropic contributions of selected SAXS images. (C) The visually enhanced equatorial streak feature of selected SAXS image.

Figure 5B shows that in zone-III the crystallinity still increases with strain, but at a much reduced rate. This indicates the retardation of strain-induced crystallization. The decreasing crystallization rate is due to the reduction of available space for strain-induced crystallization in this zone. It should be pointed out that the crystallinity at this point was only 10%, and there should be enough space for crystallization. However, if the crystallization could only occur in microfibrils, the limited space would slow down the crystallization rate. Thus, we hypothesize that in zone II the energy absorbed by the sample is mainly used for formation of superstructure (microfibril and lamellar morphology) due to crystallization, while in zone III, the energy absorbed by the sample is mainly used for structural destruction, such as the splitting of microfibrils and the distortion of lamellar structure (as seen by the conversion of a four-point pattern to a two-bar pattern in SAXS). In addition, we observed another meridional scattering having a triangle shape at low angles. The corresponding long period of this pattern near the beam stop was about 100 nm, indicating a large periodic superstructure. This scattering feature suggests the occurrence of microfibrillar splitting or newly developed aggregation of crystallites. Because the appearance of the superstructure coincided with the reduction of crystallization rate and the decrease of equatorial long period, we favor the possibility of structural destruction. In Figure 2, it is interesting to note that WAXD patterns in zone III still exhibited an intense amorphous halo, indicating the persistence of some isotropic amorphous chains. It is conceivable that some isotropic amorphous domains, outside the network of microfibrillar structure, did not encounter deformation even at high strains.

3.2. Deformation at 90 °C. Figure 6A illustrates in-situ SAXS images (corrected by sample thickness and background scattering) and load−strain curve of amorphous PET drawn at 90 °C; Figure 6B illustrates selected SAXS images, where the scattering contribution from nondeformed sample was subtracted; Figure 6C shows another set of selected SAXS images to reveal the evolution of equatorial scattering streak feature during deformation. The corresponding WAXD patterns and subtracted anisotropic images (i.e., with the removal of amorphous contribution) are illustrated in Figure 7. The number at the upper left on each image indicates the strain at which the image was taken. The peak assignments were given on the images of 200% and 570% strains, where the zones were also indicated. The detailed schemes for WAXD analysis to extract crystallinity and crystalline size were discussed elsewhere.[1,2] Figures 8 and 9 show the corresponding changes in long period and SAXS invariant, respectively. For the most part, the relationships between the LS responses and structure for measurements at 90 and 100 °C were quite similar. The structural formation at 90 °C is explained in this section, and the differences and similarities between 90 and 100 °C are discussed in detail in the next section.

3.2.1. Zone I: Plastic Deformation Zone (Strain 0−160%). In the load−strain curve (Figure 6A), zone I could be

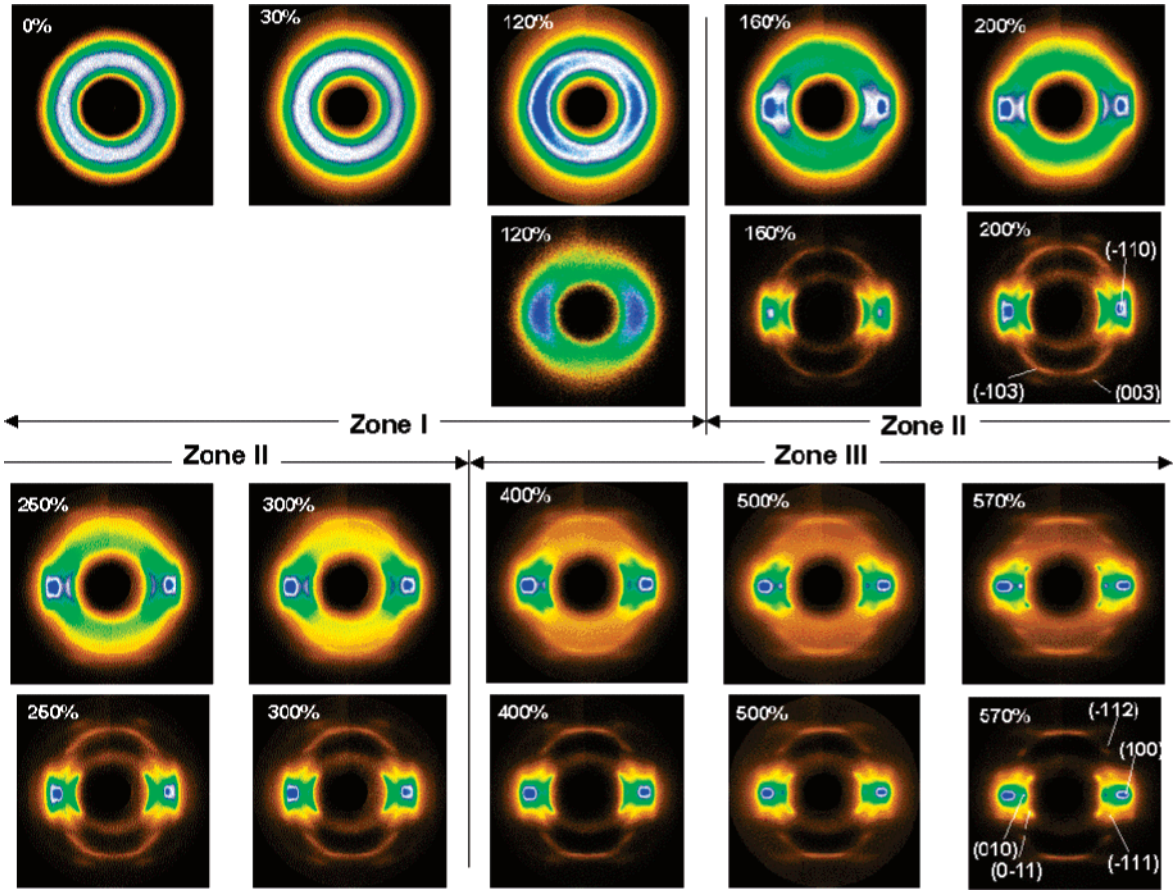

Figure 7. Selected WAXD images of the amorphous PET sample drawn at 90 °C: (upper) as measured patterns; (lower) anisotropic contributions of the images.

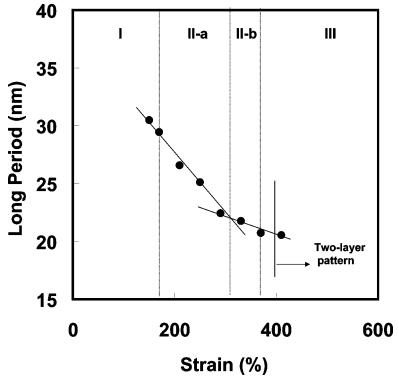

Figure 8. Long period change with strain during drawing at 90 °C.

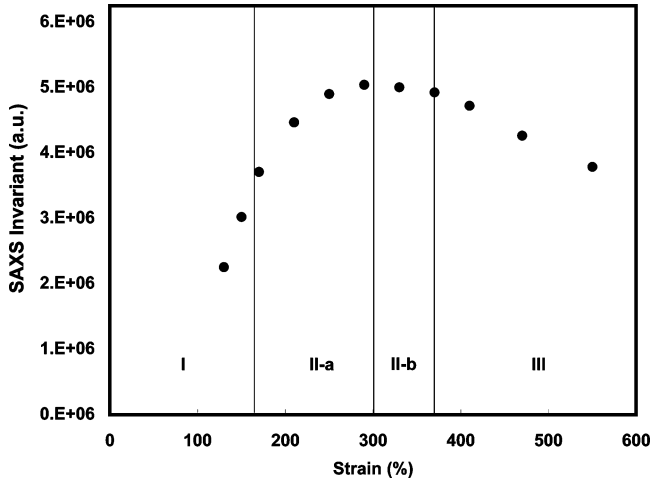

Figure 9. Invariant change from the SAXS pattern during drawing at 90 °C.

categorized in the strain region from 0 to 160%. At strains from 0 to 90%, SAXS and WAXD exhibited no scattering/diffraction signals, whereas at strains from 90 to 160%, SAXS showed a distinct equatorial streak (Figure 6C), and the corresponding WAXD also exhibited a small fraction of oriented component but still without discernible crystalline peaks (Figure 7). WAXD results indicated the possible existence of mesomorphic phase (although we could not identify the exact nature of the phase), which occurred slightly after the appearance of equatorial streak in SAXS. The equatorial streak is assigned as microfibril structure, and the microfibril is composed of the oriented mesomorphic structure as described for 100 °C.

It is interesting to note that weak but distinct X-shaped SAXS patterns were seen in the later stages of zone I (e.g., at 130% strain in Figure 6B), while these patterns did not show the scattering maximum. Corresponding WAXD patterns exhibited an oriented scattering feature around the equator but without crystal reflections, which indicated the possible formation of mesophase prior to crystallization. The oriented mesophase increased linearly in this zone before the occurrence of crystallization at 160% strain, which had also been reported earlier.[1,2] These findings are quite consistent with the mechanism of structure formation proposed as in our earlier deformation study below T_g.[3]

3.2.2. Zone II: Strain Hardening Zone (160−370%). Strain hardening began at 160% strain, where the load began to rise nonlinearly with strain. This zone could also be divided into two subzones for discussion: zone II-a (strain 160−300%) and zone II-b (strain 300−370%).

In Figure 6, it was found that in the early stage of zone II-a the SAXS pattern changed from X-shaped (e.g., 170% strain in Figure 6B) to four-point. As in the scenario at 100 °C, results at 90 °C also indicated the occurrence of microfibrils, containing lamellae with tilted arrangement, while there was no correlation among the microfibrils. The estimated tilt angle for the lamellae in the microfibril was about 67°, and the estimated lamellar dimensions were as follows: the size along the plane normal of the (100) reflection was 2.0−2.5 nm, and that of the (010) reflection was about 4.0 nm. The quantitative results (i.e., long period and invariant) from the SAXS measurements are shown in Figures 8 and 9, respectively. The long period was found to decrease more rapidly in zone II-a than in zone II-b. However, Figure 9 indicates that although the invariant increased in zone II-a, it became saturated in zone II-b. The decrease in long period, the increase in invariant, and the increase in crystallinity[1,2] all suggested the process of lamellar insertion, which has been discussed in section 3.1.2. In addition, we hypothesize that the slipping of benzene molecule could take place in imperfect triclinic crystallites,[1] and the subsequent perfection process would decrease the corresponding *d* spacings in the crystallites.[2]

The lamellar insertion process appeared to slow down in zone II-b, resulting in deceleration of the decrease in long period. The corresponding crystallinity still increased linearly in this subzone,[1,2] but the invariant reached a plateau value. The invariant saturation may be due to the decrease of scattering contrast in the microfibril. In other words, the average density of the microfibril increased with strain, caused mainly by the increase of molecular packing in the noncrystalline domain, while the increase in the crystalline density (due to crystal perfection) was relatively smaller. A similar behavior was also seen at 100 °C.

3.2.3. Zone III: Linear Load−Strain Relationship (>370%). In zone III, the distinct four-point SAXS feature was found to diminish, and an intense two-point feature along the meridian with scattering maximum near the beam stop began to appear (Figure 6C). The appearance of the equatorial streak seemed to remain constant with increasing strain. The long period of the four-point pattern changed slightly from 20 to 17 nm, but the long period of the newly developed two-point pattern near the beam stop was about 100 nm. Such a large periodic superstructure has been observed before during the deformation of PET at 100 °C and below T_g.[3] The variations of crystallinity and unit cell parameters in this region were small,[1,2] suggesting that the observed structure changes were mainly due to the crystalline rearrangement rather than further crystallization. Judging from the decrease in the SAXS invariant, the density difference between crystalline and noncrystalline regions in microfibrils continued to decline.

3.3. Mechanism for Evolution of Superstructure and Relationship with Mechanical Response. The mechanism of strain-induced phase transition and its relationship with superstructure formation in PET during deformation below T_g has been proposed by us before.[3] In the current study (deformation above T_g), the strain-induced phase transition involving mesophase(s) is significantly weakened because the increased chain mobility facilitates direct crystallization without forming detectable metastable mesophase(s) first. The evolution of superstructure above T_g (i.e., without or under the small influence of mesophase transition) appears to be similar to that below T_g, (i.e., under the large influence of mesophase transition). In summary, the load−strain curve can be divided into three zones (plastic deformation zone, strain hardening zone, and linear load increase zone), where the corresponding mechanism for each zone is outlined as follows by comparison of similarity and difference between the superstructure formations at 100 and 90 °C (as shown in parts A and B of Figure 10, respectively).

3.3.1. Zone I: Plastic Deformation Zone. At 90 and 100 °C, SAXS showed a distinct equatorial streak in the late stages of zone I, indicating the formation of strain-induced microfibrillar structure. The corresponding WAXD also exhibited oriented features but no crystal reflections. This suggests that the polymer chains in the microfibrillar domain are oriented and may be even in the mesomorphic phase, but they are relatively homogeneous without being arranged into a periodic structure (i.e., lamellar structure). The strain region for the existence of microfibrils in zone I at lower temperatures (e.g., 90 °C: 90−160% strain) was significantly broader than that at higher temperatures (e.g., 100 °C: 160−170% strain). This indicates that the metastability of strain-induced mesophase is enhanced by the lowering of temperature. (Although we did not detect any apparent mesomorphic structure by WAXD, the oriented feature was more enhanced at 90 °C than at 100 °C.) In other words, the high mobility in polymer chains probably decreases the metastability of strain-induced mesophase at high temperatures, thus minimizing the window for mesophase formation. This hypothesis is consistent with our earlier study below T_g.[3] The induction of microfibrillar structure is not directly related to strain-induced crystallization, but it appears to be associated with the phase transition between the amorphous and mesomorphic states. Generally speaking, at lower temperatures, the existence of strain-induced mesomorphic transition becomes more favorable due to the enhanced metastability, whereas at higher temperatures, the mesomorphic phase is not apparent because the transition from mesophase to crystalline can be very fast. It seems that crystallization occurs mainly within the microfibrillar domain (Figure 10), serving as the precursor state for the formation of three-dimensional crystalline ordering.

Schultz et al. predicted the presence of continuous scattering from the origin of the *q*-axis caused by sporadic nucleation.[50,51] They showed that the scattering near zero angle could be observed for slit-smearing scattering from a finite perfect stack of lamellae, and the "spike" (or low-angle up-turn) would remain even with the increase of the number of lamellae stacks. In zone I, we observed the similar diffuse scattering upturn near the beam stop even in the presence of the X-shaped pattern. This indicates that the formation of well-ordered lamellar stacks through sporadic nucleation might occur in this stage. From the standpoint of the relationship between the microfibrillar structure and mechanical property, the development of microfibrils does not always correspond to the onset of the load rise.

3.3.2. Zone II: Strain Hardening Zone. On the basis of combined SAXS and WAXD results, we hypothesize that crystallization takes place in the microfibril domain through a sporadic nucleation process during deformation. The higher the temperature, the greater the strain required to induce crystallization (Figure 10A). The change of superstructure and the relationship with crystallization can be described as follows. In zone II-a, SAXS exhibited first an X-shaped pattern (without the scattering maximum) and then a distinct four-point pattern (with the scattering maximum) having the principal axis of scattering peak oriented along the scattering arm. The corresponding WAXD showed the appearance of crystalline reflections, which gradually changed with strain.[1,2] The crystallinity at both temperatures increased continuously (Figure 5B). These results indicate that the growth of the nuclei is rapid and directional, resulting in the formation of lamellae with their principal axis tilted against the stretching direction (Figure 10).

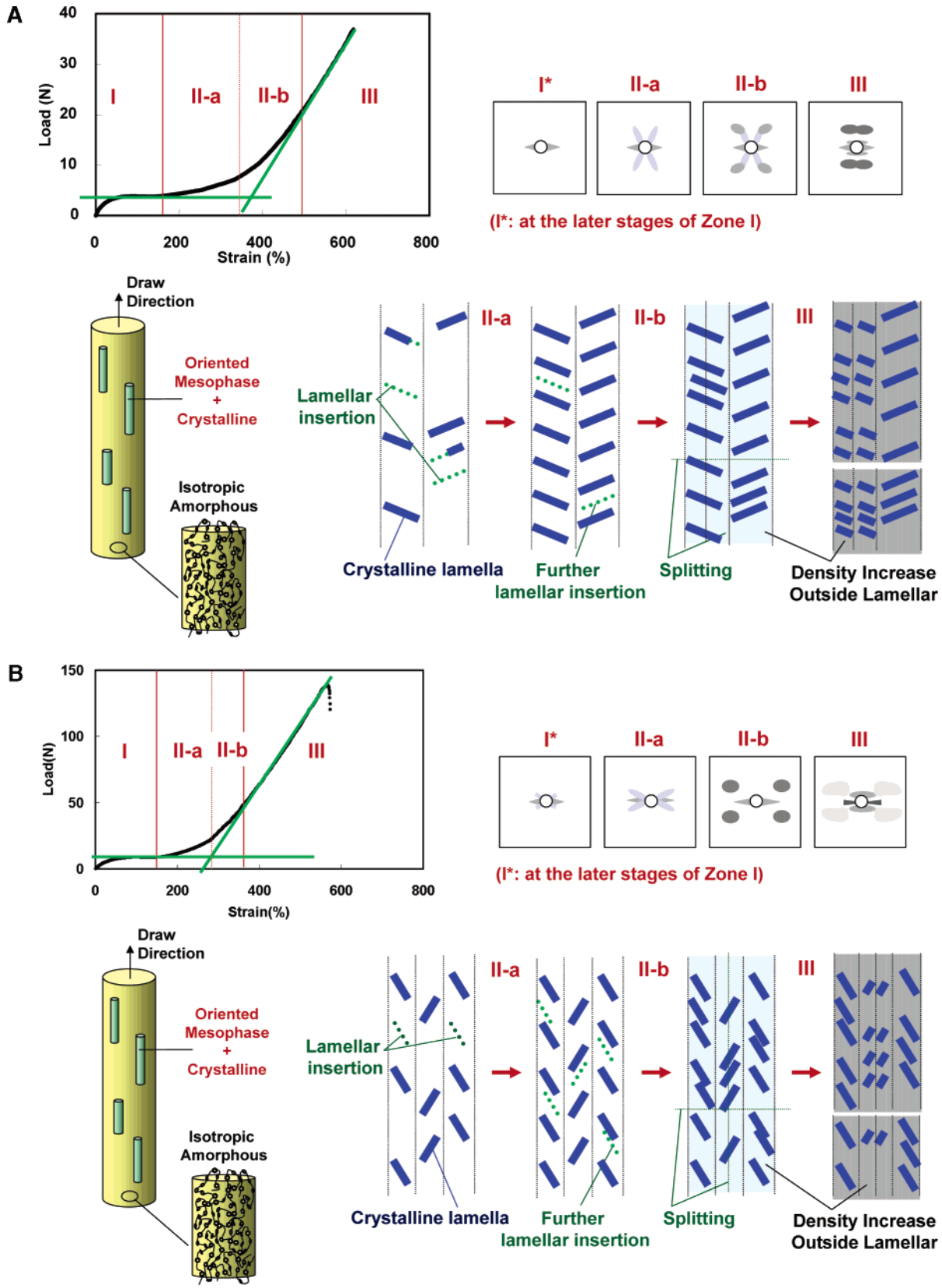

Figure 10. Schematic diagrams to illustrate the evolution of superstructure during deformation of amorphous PET sample above T_g: (A) drawing at 100 °C; (B) drawing at 90 °C. The background color of the microfibril is varied from white to dark gray gradually. The darkness represents the density of the region (darker color indicates higher density). The microfibril is composed of oriented mesophase and tilted crystalline lamellae.

The tilted lamellar structure is the result of specific chain registrations from the formation of monoclinic cell, where benzene stacking can slip past each other with strain during stretching due to local shearing motion.[1,2] The growth of sporadically nucleated lamellae leads to the formation of a three-dimensional crystalline network, which causes the load to increase significantly. Some stretched chains are imbedded in the microfibrils, and other stretched chains interconnect the microfibrils. The former can reinforce the microfibrils through the three-dimensional crystalline network; the latter can restrict

the motion of microfibrils, resulting in further load enhancement. The rapid decrease in long period with strain in zone II-a is due to the lamellar insertion mechanism, which originated from the sporadic nucleation process. In zone II-b, the four-point SAXS pattern shows a rotation of the scattering peak, having the principal axis perpendicular to the stretching direction. The corresponding rate of long period decrease is reduced significantly, but the crystallinity still increases linearly with strain. These results can be explained by the continuation of lamellar insertion (Figure 10), where the influence of new crystal addition becomes much less on the average long period, but the process generates a more homogeneous chessboard-like superstructure.

Overall, there were several different features between the X-ray results from 90 and 100 °C. The first difference was that the orientation of the crystalline phase induced at 90 °C was higher than that at 100 °C. For example, the crystalline reflections (100), (010), and (−110) in the WAXD patterns at 90 °C were all located near the equator (Figure 7), which was not the case at 100 °C. This is probably caused by the slow molecular relaxation at lower temperatures. The second difference was that the tilt angles of the X-shaped arm in the SAXS pattern were quite different at two temperatures. Using the machine axis (i.e., the meridional direction) as the reference, the estimated tilt angle was about 67° at 90 °C and 25° at 100 °C. The third difference was that the scattering peak was observed at the very early stages of zone II-a at 90 °C, where it was seen only at the later stages at 100 °C. The fourth difference was that the strain-hardening region (zone II) at 90 °C was narrower than that at 100 °C (170−470%). The fifth difference was that the oriented mesophase was observed before crystallization at 90 °C but was not at 100 °C due to rapid transition from the mesophase to crystalline phase. The last difference was that the change of the crystalline size (Figure 5A) was relatively small at 100 °C compared with that at 90 °C.[2] This could be caused by rapid perfection of the crystalline phase at higher temperatures. These differences are consistent with our hypothesis that the metastability of mesophase increases at low temperatures, which facilitates the development of more oriented solid-state morphology. However, despite these differences, the mechanism of lamellar insertion induced by uniaxial deformation seems to be applicable to explain all experimental results observed at both temperatures.

3.3.3. Zone III: Linear Load Increase Zone. In this zone, crystallization slows down because the available sites for continuing nucleation and growth are significantly reduced at high strains. The corresponding changes of crystallinity and unit cell parameters are very small in this zone at both temperatures. The load may directly reflect the energy required to deform the crystalline lamellar structure with microfibrils, and it appears to increase linearly with strain. SAXS exhibited the diminishing of the four-point pattern and the appearance of a new two-point pattern at low scattering angle (near the beam stop) with a long period about 100 nm. These results suggest the occurrence of microfibrillar splitting (Figure 10), which destroys some lamellar structures. The fragmented microfibrillar domain thus may result in a large superstructure with a 100 nm spacing, which has also been observed in the deformation study below T_g.[3] There may be another possibility that some new high-density clusters with 100 nm spacing develop. However, we think this hypothesis is weak because the crystallinity and SAXS invariant did not change significantly. Thus, the microfibrillar splitting model is more consistent with the observed SAXS and WAXD results.

There are several possible reasons for the occurrence of microfibrillar splitting at high strains, such as due to structural defects in microfibrils like kinks. It is interesting to note that the initiation of the large periodic superstructure always appears at the final stage of this zone before the sample breaks. It is conceivable that the splitting of microfibril may initiate the catastrophic failure of the sample. We observed some differences between the results in this stage at 90 and 100 °C. The first difference was that the WAXD pattern at 100 °C exhibited a strong amorphous halo even at breaking, indicating the persistence of isotropic amorphous chains. On the other hand, the WAXD results at 90 °C showed much less isotropic amorphous phase. This may be because the number of chains having long relaxation time is smaller at 100 °C, more chains would remain in the isotropic state than those at 90 °C. The second difference concerned the behavior of the SAXS invariant. It was seen that at 90 °C the scattering invariant significantly decreased, indicating that the density contrast between the crystalline lamellae and the surroundings was smaller than that at 100 °C.

4. Conclusions

The evolution of superstructure and its relationship with strain-induced phase transition during uniaxial deformation of amorphous PET at temperatures (90 and 100 °C) above T_g was investigated by means of in-situ SAXS and WAXD techniques. Results indicate that the categorization of three zones to relate to the structure and mechanical properties is applicable to temperatures below and above T_g. The change of temperature significantly alters the stability of the strain-induced mesophase, but it does not affect the evolution of superstructure, except for the strain range related to the appearance of these three zones. In zone I (plastic deformation zone), no identifiable structure and mesophase are seen at the early stages of deformation, whereas a distinct microfibrillar superstructure (the equatorial streak from SAXS) coupled with oriented chain conformation appears at the later stages. The decrease in temperature can significantly enhance the stability of oriented mesophase. In zone II (strain hardening zone), crystallization takes place in the microfibrillar domain, resulting in formation of a network linked by tilted lamellae. The increasing strain induces further nucleation and growth, leading to the process of lamellar insertion, which profoundly affects the resulting SAXS pattern (e.g., from X-shaped to four-point) and lamellar long period. In zone III (linear load zone), the saturated lamellar superstructure is responsible for the linear load increase. However, at very high strains, some lamellar domains become fragmented, resulting in microfibrillar splitting and the prelude for catastrophic breakage.

Acknowledgment. The authors thank the Toray Industries in Japan and the National Science Foundation (DMR-0405432) for the financial support of this study. The authors also thank Mr. Uchida from Toray for the synthesis of experimental PET samples.

References and Notes

(1) Kawakami, D.; Hsiao, B. S.; Ran, S.; Burger, C.; Fu, B.; Sics, I.; Hsiao, B. S. *Macromolecules* **2003**, *36*, 9275.
(2) Kawakami, D.; Ran, S.; Burger, C.; Fu, B.; Sics, I.; Chu, B.; Kikutani, T. *Polymer* **2004**, *45*, 905.
(3) Kawakami, D.; Hsiao, B. S.; Burger, C.; Ran, S.; Avila-Orta, C.; Sics, I.; Kikutani, T.; Chu, B. *Macromolecules* **2005**, *38*, 91.
(4) Ran, S.; Wang, Z.; Burger, C.; Chu, B.; Hsiao, B. S. *Macromolecules* **2002**, *35*, 10102.
(5) Asano, T.; Balta-Calleja, F. J.; Flores, A.; Tanigaki, M.; Mina, M. F.; Sawatari, C.; Itagaki, H.; Takahashi, H.; Hatta, I. *Polymer* **1999**, *40*, 6475.
(6) Welsh, G. E.; Blundell, D. J.; Windle, A. H. *Macromolecules* **1998**, *31*, 7562.

(7) Welsh, G. E.; Blundell, D. J.; Windle, A. H. *J. Mater. Sci.* **2000**, *35*, 5225.
(8) Blundell, D. J.; Mahendrasingam, A.; Martin, C.; Fuller, W. *J. Mater. Sci.* **2000**, *35*, 5057.
(9) Mahendrasingam, A.; Blundell, D. J.; Martin, C.; Fuller, W.; MacKerron, D. H.; Harvie, J. L.; Oldman, R. J.; Riekel, C. *Polymer* **2000**, *41*, 7803.
(10) Blundell, D. J.; Mahendrasingam, A.; Martin, C.; Fuller, W.; MacKerron, D. H.; Harvie, J. L.; Oldman, R. J.; Riekel, C. *Polymer* **2000**, *41*, 7793.
(11) Mahendrasingam, A.; Martin, C.; Fuller, W.; Blundell, D. J.; Oldman, R. J.; MacKerron, D. H.; Harvie, J. L.; Riekel, C. *Polymer* **2000**, *41*, 1217.
(12) Blundell, D. J.; MacKerron, D. H.; Fuller, W.; Mahendrasingam, A.; Martin, C.; Oldman, R. J.; Rule, R. J.; Riekel, C. *Polymer* **1996**, *37*, 3303.
(13) Mahendrasingam, A.; Blundell, D. J.; Wright, A. K.; Urban, V.; Narayanan, T.; Fuller, W. *Polymer* **2003**, *44*, 5915.
(14) Chaari, F.; Chaouche, M.; Doucet, J. *Polymer* **2003**, *44*, 473.
(15) Fukao, K.; Koyama, A.; Tahara, D.; Kozono, Y.; Miyamoto, Y.; Tsurutani, N. *J. Macromol. Sci., Phys.* **2003**, *B42*, 717.
(16) Radhakrishnan, J.; Kaito, A. *Polymer* **2001**, *42*, 3859.
(17) Salem, D. R. *Polymer* **1992**, *33*, 3182.
(18) Salem, D. R. *Polymer* **1992**, *33*, 3189.
(19) Gorlier, E.; Haudin, J. M.; Billion, N. *Polymer* **2001**, *42*, 9541.
(20) Bonart, R. *Kolloid-Z.* **1966**, *213*, 1.
(21) Shimizu, J.; Kikutani, T.; Takaku, A.; Okui, N. *Sen'i Gakkaishi* **1981**, *37*, T-135.
(22) Shimizu, J. *Sen'i Gakkaishi* **1985**, *38*, 243.
(23) Kubo, H.; Okamoto, M.; Kotaka, T. *Polymer* **1998**, *39*, 4827.
(24) Ran, S.; Zong, X. H.; Fang, D. F.; Hsiao, B. S.; Chu, B.; Ross, R. *J. Appl. Crystallogr.* **2000**, *33*, 1031.
(25) Chu, B.; Hsiao, B. S. *Chem. Rev.* **2001**, *101*, 1727.
(26) Ran, S.; Fang, D.; Zong, S.; Hsiao, B. S.; Chu, B.; Cunniff, P. M. *Polymer* **2000**, *42*, 1601.
(27) Hsiao, B. S.; Chu, B. Scattering: Light, Neutrons and X-rays. In *Encyclopedia of Chemical Physics and Physical Chemistry*; Institute of Physics Publishing: London, 2001; B1.9, Vol. 12, p 1197.
(28) Mendelson, A. *Plasticity: Theory and Application*; Kreiger: Huntington, NY, 1983.
(29) Lubliner, J. *Plasticity Theory*; Prentice-Hall: Upper Saddle River, NJ, 1998.
(30) Hill, R. *Mathematical Theory of Plasticity*; Oxford University Press: New York, 1998.
(31) Cakmak, M.; Teitge, A.; Zachmann, H. G.; White, J. L. *J. Polym. Phys., Polym. Phys.* **1993**, *31*, 371.
(32) Samon, J. M.; Schultz, J. M.; Hsiao, B. S.; Seifert, S.; Stribeck, N.; Gurke, I.; Saw, C.; Collins, G. *Macromolecules* **1999**, *32*, 8121.
(33) Schultz, J. M.; Hsiao, B. S.; Samon, J. M. *Polymer* **2000**, *41*, 8887.
(34) Terrill, N. J.; Fairclough, P. A.; Towns-Andrews, E.; Komanschek, B. U.; Young, R. J.; Ryan, A. *Polymer* **1998**, *39*, 2381.
(35) Olmsted, P. D.; Poon, W. C. K.; Mcleish, T. C. B.; Terrill, N. J.; Ryan, A. *Phys. Rev. Lett.* **1998**, *81*, 373.
(36) Somani, R. H.; Yang, L.; Hsiao, B. S.; Agarwal, P.; Fruitwala, H.; Tsou, A. H. *Macromolecules* **2002**, *35*, 9096.
(37) Yang, L.; Somani, R. H.; Sics, I.; Hsiao, B. S.; Kolb, R.; Fruitwala, H.; Ong, C. *Macromolecules* **2004**, *37*, 4845.
(38) Schultz, J. M.; Lin, J. S.; Hendricks, R. W.; Petermann, J.; Gohil, R. M. *J. Polym. Sci., Polym. Phys. Ed.* **1981**, *19*, 609.
(39) Petermann, J.; Schultz, J. M. *J. Mater. Sci.*. **1978**, *13*, 2188.
(40) Imai, M.; Mori, K.; Mizukami, T.; Kaji, K.; Kanaya, T. *Polymer* **1992**, *33*, 4451.
(41) Imai, M.; Mori, K.; Mizukami, T.; Kaji, K.; Kanaya, T. *Polymer* **1992**, *33*, 4457.
(42) Imai, M.; Kaji, K.; Kanaya, T. *Macromolecules* **1994**, *27*, 7103.
(43) Imai, M.; Kaji, K.; Kanaya, T.; Sakai, Y. *Physica B* **1995**, *213 & 214*, 718.
(44) Imai, M.; Kaji, K.; Kanaya, T. *Phys. Rev. Lett.* **1993**, *71*, 4162.
(45) Imai, M.; Kaji, K.; Kanaya, T.; Sakai, Y. *Phys. Rev. B* **1995**, *52*, 12 696.
(46) Somani, R. H.; Hsiao, B. S.; Nogales, A.; Srinivas, S.; Tsou, A. H.; Sics, I.; Balta-Calleja, F. J.; Ezquerra, T. A. *Macromolecules* **2000**, *33*, 9385.
(47) Fischer, E. W.; Fakirov, S. J. *J. Mater. Sci.* **1976**, *11*, 1041.
(48) Goschel, U. *Polymer* **1995**, *36*, 1157.
(49) Goschel, U.; Deutscher, K.; Abez, V. *Polymer* **1996**, *37*, 1.
(50) Schultz, J. M. *J. Polym. Sci.*. **1976**, *14*, 2291.
(51) Schultz, J. M.; Lin, J. S.; Hendricks, R. W. *J. Appl. Crystallogr*. **1978**, *11*, 551.

MA052589Y